# X-ray absorption and occultation in LS 5039

Anna Szostek, G. Dubus

▶ **To cite this version:**

Anna Szostek, G. Dubus. X-ray absorption and occultation in LS 5039. Monthly Notices of the Royal Astronomical Society, 2010, pp.1637. ⟨hal-00631975⟩

**HAL Id: hal-00631975**

**https://hal.science/hal-00631975v1**

Submitted on 22 Nov 2021

**HAL** is a multi-disciplinary open access archive for the deposit and dissemination of scientific research documents, whether they are published or not. The documents may come from teaching and research institutions in France or abroad, or from public or private research centers.

L'archive ouverte pluridisciplinaire **HAL**, est destinée au dépôt et à la diffusion de documents scientifiques de niveau recherche, publiés ou non, émanant des établissements d'enseignement et de recherche français ou étrangers, des laboratoires publics ou privés.

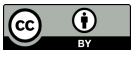

Distributed under a Creative Commons CC BY 4.0 - Attribution - International License

Monthly Notices
of the
ROYAL ASTRONOMICAL SOCIETY

Mon. Not. R. Astron. Soc. **411,** 193–199 (2011) doi:10.1111/j.1365-2966.2010.17671.x

# X-ray absorption and occultation in LS 5039

Anna Szostek[1,2]⋆ and Guillaume Dubus[1]

[1]*Laboratoire d'Astrophysique de Grenoble, UMR 5571 Université Joseph Fourier Grenoble I/CNRS, BP 53, 38041 Grenoble, France*
[2]*Astronomical Observatory, Jagiellonian University, Orla 171, 30-244 Kraków, Poland*

Accepted 2010 September 8. Received 2010 September 8. in original form 2010 June 28

**ABSTRACT**

Gamma-ray binaries are systems containing a massive star and a compact object that have been detected up to TeV energies. The high-energy emission could result from particle acceleration in the region where the stellar wind from the massive star interacts with the relativistic wind from a young pulsar. LS 5039 has the most compact orbit amongst gamma-ray binaries and its X-ray light curve shows a stable modulation synchronized with the orbital period. Photoelectric absorption of X-rays in the O star wind and occultation of the X-ray emitting region by the massive star can alter the X-ray light curve and spectrum along the orbit. Yet, the X-ray spectrum and light curve of LS 5039 do not show intrinsic absorption or X-ray eclipses. We study these effects in the framework of the pulsar wind scenario as a function of the binary inclination angle, the stellar wind mass-loss rate and the size of the X-ray emitter. An extended X-ray emission region $\gtrsim 3R_\star$ appears necessary to reconcile the pulsar wind scenario with observations.

**Key words:** binaries: close – binaries: eclipsing – stars: individual: LS 5039 – stars: mass-loss – gamma-rays: stars – X-rays: binaries.

## 1 INTRODUCTION

Gamma-ray binaries are systems containing a massive star and a compact object that emit most of their power at energies above 100 MeV. They have been detected up to very high energy (VHE) gamma-rays and are thus sites of particle acceleration up to multi-TeV energies. There are three established gamma-ray binaries, PSR B1259−63 (Aharonian et al. 2005), LS 5039 (Aharonian et al. 2006; Abdo et al. 2009b) and LS I+61 303 (Albert et al. 2006; Abdo et al. 2009a), and a candidate binary HESS J0632+057 (Aharonian et al. 2007).

The VHE emission in gamma-ray binaries is thought to be due to Compton upscattering of UV photons from the massive star by energetic electrons. Electron acceleration could take place either in a relativistic jet (microquasar scenario, Romero, Christiansen & Orellana 2005; Dermer & Böttcher 2006; Paredes, Bosch-Ramon & Romero 2006) or in the shocked wind of a young pulsar (pulsar wind scenario, Maraschi & Treves 1981; Dubus 2006), where the shock results from the interaction between the pulsar wind and the stellar wind of the companion star. The latter model is known to be operating in case of PSR B1259−63 (Tavani, Arons & Kaspi 1994; Kirk, Ball & Skjaeraasen 1999). The nature of the compact object and the electron acceleration site is uncertain in the remaining gamma-ray binaries.

⋆E-mail: aszostek@obs.ujf-grenoble.fr

Gamma-ray binaries have also been observed in X-rays where their properties differ from those of high-mass X-ray binaries (HMXB). The X-ray spectrum of gamma-ray binaries are power laws but show no apparent cut-offs up to hundreds of keV. The X-rays are thought to be due to non-thermal synchrotron or inverse Compton emission. Gamma-ray binaries also do not display X-ray outbursts and state transitions as usually seen in accreting binaries.

LS 5039 is the most compact gamma-ray binary, composed of an unknown compact object in a 3.9-d orbit around a O6.5V star (Casares et al. 2005). It has a regular behaviour in both gamma-rays and X-rays. The X-ray light curve shows an orbital modulation with a remarkable long-term stability (Hoffmann et al. 2009; Kishishita et al. 2009; Takahashi et al. 2009). The modulation is present at low(1–10 keV) and medium(10–40 keV) X-ray energies, with minimum and maximum flux at superior and inferior conjunction, respectively. The location of the minima and maxima suggest the modulation is a geometrical effect related to the orientation of the binary with respect to the observer, rather than due to physical changes taking place in the shocked winds region when the compact object travels on its elliptical orbit.

X-ray absorption in the stellar wind and occultation of the X-ray emitting region by the massive star both result in orbital modulations with the correct phases for flux minimum and maximum. However, for LS 5039 there is no evidence for an absorption excess due to the stellar wind at any orbital phase, even at superior conjunction (Takahashi et al. 2009). This has been used to argue that the X-ray emitting region must be far out from the system, where the column density of material crossed by the X-rays is small (Bosch-Ramon

© 2010 The Authors. Journal compilation © 2010 RAS

Downloaded from https://academic.oup.com/mnras/article/411/1/193/1038827 by CNRS - ISTO user on 22 November 2021

et al. 2007; Bosch-Ramon 2010). Here, we re-examine this question in detail, taking into account the 3D geometry of the interaction in the pulsar wind scenario to compute model light curves. This is used to derive constraints on the binary parameters from the lack of absorption and occultation signatures in the observed light curve.

The outline of this article is as follows. The model is described in Section 2 and applied in Section 3 to estimate the size of the X-ray emitting region based on the observed hydrogen column density. The occultation of the X-ray emitting region by the massive star is studied in Section 4. Finally, Section 5 discusses the findings and presents the conclusions.

## 2 THE GEOMETRIC MODEL

### 2.1 Shape of the shock

In the pulsar wind scenario, X-rays are emitted by particles accelerated in the shock region where the pulsar wind and the stellar wind of the massive star collide (Fig. 1). The interaction region is bounded by two termination shocks $S_\star$ and $S_\mathrm{p}$. Downstream (zones 2 and 3), two shocked winds are separated by a tangential contact discontinuity (CD). Upstream (zones 1 and 4), the winds behave as in the case of single star/pulsar. In this example, the stellar wind momentum dominates over the pulsar wind. The stagnation point $R_\mathrm{s}$ between the two winds along the line joining the stars is found by equating the ram pressures from the two winds:

$$p_\star(R_\mathrm{s}) = \frac{\dot{M}v(R_\mathrm{s})}{4\pi R_\mathrm{s}^2} = \frac{\dot{E}}{4\pi c(a-R_\mathrm{s})^2} = p_\mathrm{p}(a-R_\mathrm{s}), \tag{1}$$

where $a$ is the binary orbital separation, $\dot{M}$ is the stellar wind mass-loss rate and $\dot{E}$ is the pulsar spin-down power. The stellar wind velocity $v$ at the radial distance $r$ from the star's centre is given by a $\beta$-velocity law (Castor, Abbott & Klein 1975):

$$v(r) = v_\infty\left(1-\frac{R_\star r_0}{r}\right)^\beta, \tag{2}$$

where $r_0 = 1-(v_0/v_\infty)^{1/\beta}$ with $v_0$ the initial wind velocity, $v_\infty$ is the wind terminal velocity, $R_\star$ is the stellar radius and $\beta \approx 1$ is a parameter describing wind acceleration.

The detailed structure of the shock will depend on the momenta of the winds and on radiative cooling of the gas. Efficient cooling will tend to collapse the termination shocks on to the CD. The shock structure can also be affected by mixing instabilities at the interface and by orbital motion (e.g. Stevens, Blondin & Pollock 1992). There is no general semi-analytic description of the shock structure but a description of the CD can be obtained. The CD is defined as the surface where the perpendicular components of the ram pressures balance each other, $p_{\star\perp} = p_{\mathrm{p}\perp}$. For each point in space one can then define a dimensionless parameter,

$$\eta(r_1) \equiv \frac{\dot{E}}{\dot{M}v(r_1)c} = \frac{r_2^2\sin^2\theta_1}{r_1^2\sin^2\theta_2}, \tag{3}$$

where $\theta_1$ an $\theta_2$ are angles between the line tangential to the CD at the given point and the direction towards the star or pulsar respectively as illustrated in Fig. 1. $r_1$ and $r_2$ are distances from the star and pulsar, respectively. The value of $\eta$ at the stagnation point ($\theta_1 = \theta_2 = \pi/2$) equals

$$\eta_0 = \eta(R_\mathrm{s}) = \frac{\dot{E}}{\dot{M}v(R_\mathrm{s})c} = \frac{(a-R_\mathrm{s})^2}{R_\mathrm{s}^2}$$
$$= 0.05\left(\frac{\dot{E}}{10^{36}\,\mathrm{erg\,s^{-1}}}\right)\left(\frac{\dot{M}}{10^{-7}\,\mathrm{M_\odot\,yr^{-1}}}\right)^{-1}\left[\frac{v(R_\mathrm{s})}{10^8\,\mathrm{cm\,s^{-1}}}\right]^{-1}. \tag{4}$$

The $\eta_0$ depends on orbital phase via $v(R_\mathrm{s})$ and parametrizes the shape of the shock, which is then obtained by solving the differential equation (equation 6 in Antokhin, Owocki & Brown 2004)

$$\frac{\mathrm{d}x}{\mathrm{d}y} = \frac{1}{y}\left\{x - \frac{ar_1^2(x,y)\sqrt{\eta\,[r_1(x,y)]}}{r_1^2(x,y)\sqrt{\eta\,[r_1(x,y)]}+r_2^2(x,y)}\right\} \tag{5}$$

with the initial condition $x = R_\mathrm{s}$ and $y = 0$. Numerical simulations show that this holds reasonably well in the case of the interaction with a relativistic pulsar wind (Bogovalov et al. 2008). The solution is a 2D profile of the CD $x = f(y)$. The CD is symmetrical with respect to $x$-axis, thus it is best represented in cylindrical coordinates $(\rho, \psi, x)$ as $x = f(\rho)$, where $\rho = \sqrt{y^2+z^2}$ and $\psi = \arctan(z/y)$.

An example 3D representation of the model is shown in Fig. 2. In cases where $\eta_0 < 1$ the stellar wind dominates over the pulsar wind. When $\eta_0 \ll 1$, the opening angle of the CD $\alpha \lesssim 45^\circ$ (where $\alpha$ is an angle between $x$-axis and a line tangential to the CD at a large distance from the stagnation point) and the CD wraps around the pulsar creating a tail-like structure. For $\eta_0 > 1$ the opening angle

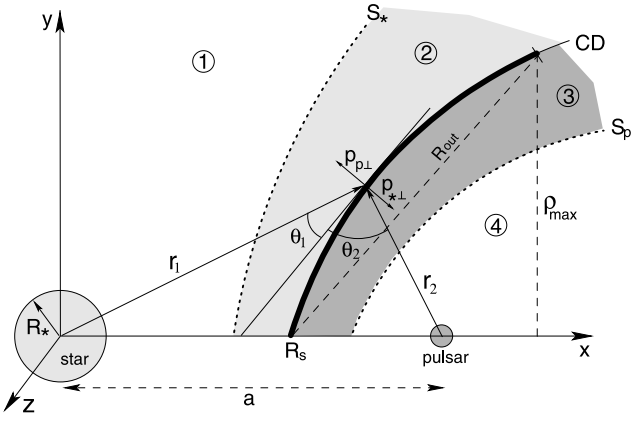


**Figure 1.** The schematic 2D illustration of the model where the stellar wind and pulsar wind collide. The sizes of the pulsar and star are not to scale.

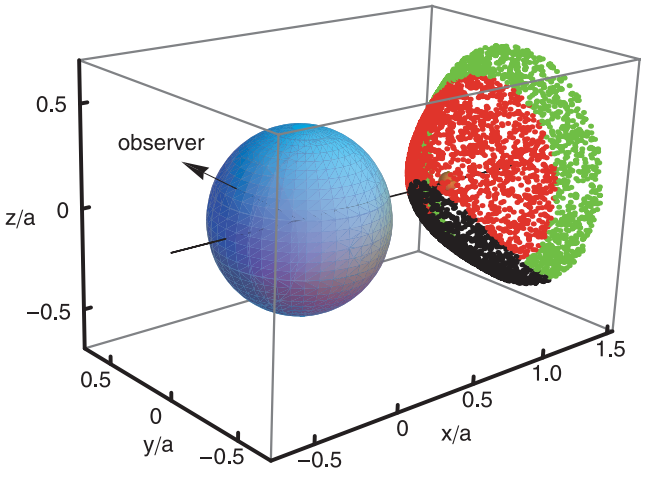


**Figure 2.** 3D illustration of LS 5039 in the framework of the pulsar wind scenario. The plot is in units of orbital separation and the massive star is plotted to scale. The dark sphere is the massive star, the light grey (green) points represent the CD surface, the dark grey (red) points are the points that emit X-rays, whereas black points are in the shadow of the massive star. The arrow represents the direction to the observer at inclination 60° and at the phase of superior conjunction.

Downloaded from https://academic.oup.com/mnras/article/411/1/193/1038827 by CNRS - ISTO user on 22 November 2021

$\alpha > 90^\circ$ and the CD curves around the massive star. Note that there is a maximum value of $\eta_0$ associated with a minimum realizable distance $R_s^{\min}$ between the star and CD. This is approximately the place where $p_\star(r)$ has its maximum. Stable balance is lost if the pulsar wind moves beyond this point: then the pulsar wind overwhelms the stellar wind and is stopped at the star surface.

The shape of the CD will be correct up to the point where the Coriolis force curves the shock structure. Assuming that the stellar wind is collimating the pulsar wind, this happens at a distance $\sim v_\infty P_{\rm orb}$, or about 5.4 au (130 $R_\star$) for LS 5039 with the parameters given in Section 2.4. Closer in, the orientation of the surface can also be altered by orbital motion: the skew angle $s$ is given by $\tan s = v_{\rm orb}/v(a)$ where $v_{\rm orb}$ is the pulsar orbital velocity.

### 2.2 X-ray emission

In the pulsar wind scenario, the X-ray emission is primarily due to synchrotron emission in the shocked pulsar wind region (zone 3 in Fig. 1) which is tenuous and optically thin to X-rays. The stellar wind region may also be a source of X-rays, either because of the kinetic energy dissipated in the colliding winds (zone 2) or due to small-scale instabilities in the stellar wind (zone 1) (Puls, Vink & Najarro 2008). In both cases the emission is softer ($kT \approx$ 0.5 keV) and weaker ($10^{30}$–$10^{33}$ erg s$^{-1}$, e.g. Stevens et al. 1992) than the observed X-ray emission from LS 5039 ($\approx 10^{33}$ erg s$^{-1}$, Takahashi et al. 2009). Detecting X-ray line emission would provide valuable diagnostics of the stellar wind but this emission is most likely swamped by synchrotron emission.

The cooling parameter $\chi \equiv t_{\rm cool}/t_{\rm dyn}$ of the O star wind (Stevens et al. 1992) is $\approx$1 in LS 5039, at the limit of efficient radiative cooling. Isothermal (radiatively efficient) shocks have small widths. The pressure in the shocked pulsar wind will mostly be due to the lowest-energy electrons if the particles have a steep distribution. These electrons have long cooling times and the shock may be more closely approximated as adiabatic rather than isothermal. Complex numerical simulations are required to obtain the detailed structure and emissivity of the shock region. At this stage, we assume that the shocked regions 2 and 3 have a negligible width and that the emissivity is uniform over the 2D shock surface, which should suffice to capture the geometrical effects that we want to investigate.

The emitting 2D shock surface is approximated by the CD surface for $\rho \in \langle 0, \rho_{\max}\rangle$ and, with $\rho_{\max}$ the cylindrical radius at which a sphere centred at ($R_s$, 0, 0) of radius $R_{\rm out}$ intersects the CD (see Fig. 1). The size of the emitting region is conveniently parametrized by $R_{\rm out}$ in the following. The total flux from the emitting volume is

$$F(E) = \int_V j_{\rm E}{\rm d}V = \int_S \lambda\ j_{\rm E}{\rm d}S, \tag{6}$$

where $j_{\rm E}$ is the unit volume emissivity and $\lambda j_{\rm E}$ is the constant surface emissivity. The unit surface element of CD equals

$$dS = \sqrt{1 + \left(\frac{\partial f}{\partial \rho}\right)^2}\ \rho\ {\rm d}\rho\ {\rm d}\psi. \tag{7}$$

### 2.3 Absorption and occultation

The uniform emission of X-rays is affected in two, orbital phase-dependent, ways. First, X-rays can undergo photoelectric absorption as they cross the dense stellar wind. The wind density at the distance $r$ from the stellar centre is

$$n(r) = \frac{\dot{M}}{4\pi\mu m_{\rm H} r^2 v(r)}, \tag{8}$$

where $m_{\rm H}$ is hydrogen mass while $\mu = 1.3$ is the mean molecular weight. Second, at some phases and for some inclinations, parts of the emitting surface of the CD are occulted by the massive star and are thus invisible to the observer (black regions in Fig. 2).

In order to estimate the impact of absorption and occultation on the observed flux, a random sample of $N$ points is uniformly distributed on the surface of CD out to $R_{\rm out}$ (see Fig. 2 and Appendix A). Each point corresponds to an $N$th part of the emitting surface and has a flux equal to $1/N$ (the total flux is normalized to unity). The observed flux at given energy $E$, inclination angle $i$ and orbital phase $\phi$ is

$$F(E, i, \phi) = \frac{1}{N}\sum_{j=1}^{N} \exp[-\sigma(E) N_{{\rm H}j}(i, \phi)]\ \zeta_j(i, \phi), \tag{9}$$

where $N_{{\rm H}j}$ is the stellar wind's hydrogen column density obtained from integration of $n(r)$ along the line of sight from point $j$ and $\sigma$ is the photoelectric cross-section of the plasma which is a function of photon energy $E$. If the plasma is ionized, $\sigma$ also depends on plasma ionization parameter which varies along the line of sight. $\zeta_i$ is the occultation function of which the value is 0 whenever a line of sight crosses the interior of the massive star and 1 otherwise.

In calculations of $N_{\rm H}$ the parts of the line of sight that cross the pulsar side of the CD (zones 3 and 4 in Fig. 1) are considered to be empty since neither unshocked nor shocked pulsar wind has sufficient densities to absorb X-rays. For simplicity, we also assume that zone 1+2 are described by equation (2) all the way from the stellar surface out to the CD i.e. we ignore the density enhancement in the shocked stellar wind (zone 2). Again (Section 2.2), detailed numerical simulations would be required to model this appropriately. An estimate can be derived using the thin shell colliding wind model of Canto, Raga & Wilkin (1996). The surface density of the shock is $\approx 3\dot{M}\sqrt{\eta}/(16\pi a v)$ in the orbital plane, where it is maximum. This corresponds to a column density across the shock $N_{\rm H,shock} \approx 7 \times 10^{19} \dot{M}_{10^{-7}\,{\rm M}_\odot\,{\rm yr}^{-1}} \eta_{0.01}^{1/2} a_{0.1\ {\rm au}}^{-1} v_{2000\,{\rm km\,s^{-1}}}\,{\rm cm}^{-2}$, compared to the wind column density $N_H \approx 2 \times 10^{21}\,{\rm cm}^{-2}$ from $R_\star$ to infinity (for the same wind parameters). $N_{\rm H,shock}$ is also about 30 times less than the inferred wind column density at a superior conjunction (see Section 3). We conclude that taking into account the density enhancement in the shocked region is unlikely to change our results significantly.

### 2.4 Parameters for LS 5039

We adopt the following binary parameters for LS 5039: $v_\infty = 2.4 \times 10^8\,{\rm cm\,s^{-1}}$, $R_\star = 9.3\,{\rm R}_\odot$, $M_\star = 23\,{\rm M}_\odot$ and $T_\star = 3.9 \times 10^4$ K. For the wind of the massive star, we adopt $\beta = 1$ and $v_0 = 2 \times 10^6\,{\rm cm\,s^{-1}}$ (equation 2). The value of $\dot{M}$ in LS 5039 is not well constrained and varies from $\sim 3 \times 10^{-8}$ to $7.5 \times 10^{-7}\,{\rm M}_\odot$ yr$^{-1}$, with values of several $10^{-7}$ ${\rm M}_\odot$ yr$^{-1}$ favoured in the most recent literature (Kudritzki & Puls 2000; McSwain & Gies 2002; McSwain et al. 2004; Casares et al. 2005; Szalai, Kiss & Sarty 2010). These mass-loss rates are derived from H$\alpha$ line fitting, a diagnostic which is known to be affected by wind clumping (Puls et al. 2008). The true $\dot{M}$ could be a factor of 2–3 lower than the $\dot{M}$ estimated from H$\alpha$. The large range of $\eta_0$ that we explore covers this uncertainty.

The binary inclination angle is $i \gtrsim 40^\circ$ if the binary contains a neutron star. The orbit eccentricity is $e = 0.33$, while the angle of the line of nodes is $\omega = 236^\circ$ (Aragona et al. 2009). For these orbital parameters the periastron, apastron, pulsar superior and inferior conjunction correspond to orbital phases $\phi = 0$, 0.5, 0.045 and 0.67, respectively. The respective binary separations are

Downloaded from https://academic.oup.com/mnras/article/411/1/193/1038827 by CNRS - ISTO user on 22 November 2021

$1.4 \times 10^{12}, 2.82 \times 10^{12}, 1.46 \times 10^{12}$ and $2.59 \times 10^{12}$ cm. The skew angle is $s = 23^\circ$ at periastron and $8^\circ$ in apastron. This has a negligible impact on the conclusions and is not taken into account.

A strict lower limit on the value of $\dot{E}$ in LS 5039 is $\simeq 10^{35}$ erg s$^{-1}$ which implies 100 per cent radiative efficiency to gamma-rays (at a distance of 2–3 kpc). At the other end of the scale, the pulsar wind will impact the star surface beyond a certain $\dot{E}_{\rm max}$ set by $\dot{M}$ and the binary separation at periastron. Such a situation is thought to occur in the black widow pulsars where the wind from the low-mass stellar companion is very weak (Phinney et al. 1988). If the pulsar wind is dominated by the kinetic energy of the cold $e^+e^-$ pairs then radiative braking of the pulsar wind by inverse Compton losses might still allow a shock to form just above the O star surface (Cerutti, Dubus & Henri 2008). The magnetic field of the O star may also be sufficient to hold off the pulsar wind (Harding & Gaisser 1990). However, there is no observational evidence that the stellar wind in LS 5039 collapses due to the relativistic wind momentum impinging on its pulsar-facing hemisphere. McSwain et al. (2004) find no differences in UV spectra taken at two different orbital phases (0.40 and 0.63 based on ephemeris of Aragona et al. 2009), the latter one close to inferior conjunction of the compact object where the effect of the O star wind quenching by the pulsar wind should be most visible. Assuming that the O star wind does not collapse implies a maximum $\eta_{\rm max} \simeq 0.6$, reached at periastron, for which the CD opening angle is $\approx 62^\circ$. For the lower and upper limit on $\dot{M}$, the corresponding $\dot{E}_{\rm max}$ varies between $\sim 1.5 \times 10^{36}$ erg s$^{-1}$ and $3.8 \times 10^{37}$ erg s$^{-1}$, respectively, well below the $\dot{E}$ of the Crab pulsar ($4.6 \times 10^{38}$ erg s$^{-1}$). In the following calculations we often use the value of $\eta_0 = 0.004$ to examine the model predictions in the case of extreme stellar wind domination over the pulsar wind. At this value of $\eta_0$ the CD opening angle is only $\sim 10^\circ$.

There is also no evidence for X-ray ionization of the stellar wind (McSwain et al. 2004), suggesting that the impact of ionization on X-ray absorption can be neglected. We confirmed the validity of this assumption for LS 5039 with the photoionization code XSTAR (Kallman 2005). In the simulation, an optically thin plasma cloud was illuminated by a source with a spectrum composed of a power law with spectral index of 1.5 and 1–10 keV luminosity of $6.03 \times 10^{33}$ erg s$^{-1}$ (Takahashi et al. 2009, assuming a 2.5 kpc distance to LS 5039 from the Earth); and a blackbody (stellar continuum) with a temperature of $T_\star$, radius of $R_\star$ and luminosity of $L_\star = 6.9 \times 10^{38}$ erg s$^{-1}$. The measured opacities in the 1–10 keV range did not differ from those of the cold plasma described by Morrison & McCammon (1983). The intense UV radiation of the massive star does not influence the plasma opacity at energies above 0.5 keV.

## 3 X-RAY ABSORPTION IN LS 5039

Observations show no signatures of X-ray absorption by the stellar wind in LS 5039. The *XMM–Newton* and *Suzaku* spectra of LS 5039 are absorbed by an equivalent hydrogen column density consistent with the Galactic value. The upper limit on the intrinsic column density at the phase of superior conjunction (where the line-of-sight column density related to the stellar wind is highest) is as low as $N_{\rm H}^{\rm max} = 2.6 \times 10^{21}$ cm$^{-2}$ (Bosch-Ramon et al. 2007; Takahashi et al. 2009).

The photoelectric absorption depends on four parameters, $\dot{M}$, $i$, $R_{\rm out}$ and $\eta_0$. This can be used to estimate the maximum allowed $\dot{M}_{\rm max}$ for which the line-of-sight column density does not exceed $N_{\rm H}^{\rm max}$. For example, for a point X-ray source located at the pulsar position, at the phase of superior conjunction and at inclination angle $i = 40^\circ$, the upper limit on the stellar wind mass-loss rate is $\dot{M}_{\rm max} = 7.3 \times 10^{-8}\,{\rm M}_\odot$ yr$^{-1}$. For a point source located at the stagnation point, the $\dot{M}_{\rm max}$ is lower, since the line of sight probes regions of the stellar wind with higher density. For an X-ray emitting point source located at $R_{\rm s}$ and for which $\eta_0 = \eta_{\rm max}$, then $\dot{M}_{\rm max} = 2.3 \times 10^{-8}\,{\rm M}_\odot$ yr$^{-1}$.

These values of $\dot{M}_{\rm max}$ are at the lower end of the $\dot{M}$ scale for the Galactic O stars, ($\sim 10^{-8}$–$10^{-6}$ ${\rm M}_\odot$ yr$^{-1}$, e.g. Mokiem et al. 2007). $\dot{M}_{\rm max}$ could be higher if the wind was highly ionized but this is unlikely (see Section 2.4). $\dot{M}_{\rm max}$ could also be higher if the X-ray emitter is away from the massive star, e.g. in the form of a jet, emitting X-rays at a distance $>10^{12}$ cm where the stellar wind is rarified (Bosch-Ramon et al. 2007). Another possibility is that the X-ray emitting region is not point-like but large compared to the size of the massive star.

For the measured value of $N_{\rm H}^{\rm max}$ and as a function of $\dot{M}_{\rm max}$, we estimate the minimum size of the X-ray emitting region for which intrinsic absorption would not manifest itself in the X-ray spectrum. The upper limit $N_{\rm H}^{\rm max}$ is based on X-ray data fitting which assumed that an entire (point or extended) X-ray source is covered by a uniform absorbing gas cloud so that

$$F(E) = \exp[-\sigma(E) N_{\rm H}], \tag{10}$$

where the intrinsic flux equals 1. In our case, however, where an extended X-ray source is absorbed by a stellar wind, the line-of-sight column density of each X-ray emitting surface element is different and the observed flux is given by equation (9). In general, the observed spectra of a source covered by an uniform absorber and of a source covered by stellar wind are different ($\lesssim$5 keV). We assume that the spectral fitting is not able to distinguish between different types of absorbers if the fluxes at 1 keV are equal i.e.

$$\frac{1}{N}\sum_{j=1}^{N} \exp[-\sigma(1\,{\rm keV}) N_{{\rm H}j}(i,\phi)] = \exp\left[-\sigma(1\,{\rm keV}) N_{\rm H}^{\rm max}\right], \tag{11}$$

where $\sigma(1\,{\rm keV}) = 2.4 \times 10^{-22}$ cm$^2$ (Morrison & McCammon 1983). This is justified, because at energies $\gtrsim$2 keV, the photoelectric cross-section decreases quickly and the difference between the two absorbed spectra is relatively small. Furthermore, the spectrum is most sensitive to absorption at energies $\lesssim$2 keV, but below 1 keV the sensitivity of the instruments starts to drop and the data errors increase, which may also make it difficult to distinguish between different models.

In order to obtain the lower limit on the size of the X-ray emitting region at 1 keV, we explore the parameter space ($\dot{M}$, $\eta$, $R_{\rm out}$, $i$) to find solutions that satisfy equation (11) at superior conjunction. In this calculation we reject points which are occulted by the star (adjusting $N$ accordingly) to test only the effect of absorption.

The estimated minimum size of the 1-keV X-ray source is shown in Fig. 3. The size of the emitting region must be larger to compensate for the denser gas when the mass-loss rate is increased. For $\eta_0 \simeq \eta_{\rm max}$ and at large emitter size, the results are not sensitive to inclination changes. The highly collimated pulsar wind shock ($\eta_0 \ll 1$) needs to have a large emitting surface to explain the observations.

## 4 OCCULTATION IN LS 5039

The occultation of the X-ray emitting region by the massive star does not depend on energy, thus its only signature in the spectrum is a periodic reduction in flux. The amplitude and duration of occultation depend on three main parameters, $i, \eta_0$ and $R_{\rm out}$. We find that the duration of the occultation is longest for binaries with circular orbits and where at all phases $\eta_0 > 1$ (when the CD curves around the

Downloaded from https://academic.oup.com/mnras/article/411/1/193/1038827 by CNRS - ISTO user on 22 November 2021

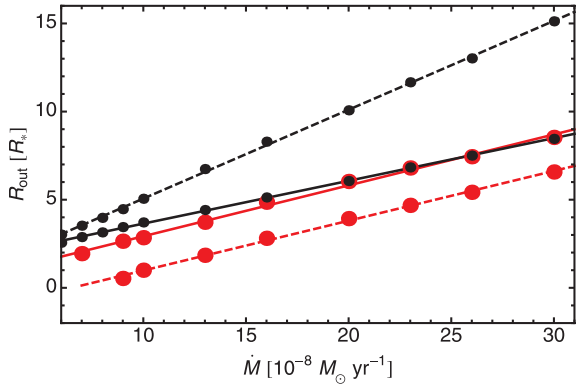


**Figure 3.** The minimum size of the X-ray 1 keV emission region at superior conjunction. The dots mark the results of calculations, the lines are linear fits to the points. The dashed lines correspond to $\eta_0 = 0.004$ at superior conjunction, the solid lines correspond to maximum value of $\eta_0 = \eta_{max} = 0.6$ at periastron. The grey (red) and black correspond to $i = 40^\circ$ and $i = 60^\circ$, respectively.

massive star). The occultation duration can last up to 40 per cent of the orbital period. The latter is because curved portions of the CD are partly occulted by the star even at phases away from the superior conjunction. The amplitude of occultation is highest if the inclination is high and the size of the emitting region is small compared to the size of the star. However, this situation is unlikely to occur in LS 5039 since $\eta_0 \lesssim 0.6$ (see Section 2.4).

When $\eta_0$ is below unity, occultation influences the shape of the X-ray light curve only around superior conjunction. Light curves calculated for the most preferable conditions to observe occultation in LS 5039 (high $\eta_0$, high $i$ and small $R_{out}$) are shown in Fig. 4(a). The dip in the light curve caused by occultation is narrow and covers only $\Delta\phi \sim 0.2$ in the phase around superior conjunction. The depth of the minimum strongly depends on $R_{out}$. Note also that for large $R_{out}$ two minima appear, separated by a local maximum. This effect is related to the size of the shadow cast by the star on to the CD surface, which is larger when the line of sight is tangential to the surface of CD. These two local minima are too narrow ($\Delta\phi \sim 0.025$) to be resolved in the *Suzaku* light curve. A similar light curve study for $\eta_0 \ll 1$ shows an even deeper and narrower minimum than in the case of $\eta_0 \sim \eta_{max}$ (Fig. 4b).

The X-ray modulation cannot be explained by occultation alone but this does not preclude an observable effect in the form of a sharp drop in flux around superior conjunction. In order to place an upper limit on this effect, we normalize the *Suzaku* light curve to 1 and fit it with a sine function in order to remove the orbital modulation. The standard deviation of the subtracted data is $\sigma_d = 0.1$. The upper limit on the depth of a dip in the data is assumed to be $3\sigma_d$, meaning a $\leq$30 per cent reduction of the 1–10 keV flux would not be statistically significant. The dip in the light curve at the superior conjunction may be caused by the combined effects of absorption and occultation. The effect of absorption on 1–10 keV flux is low. In a simple estimate, for $N_H = N_H^{max}$ and for the observed power-law spectrum of LS 5039 with photon index $\Gamma = 1.51$, the integrated absorbed (using uniform absorber, i.e. WABS model in XSPEC) 1–10 keV flux is at most ~6 per cent lower than the 1–10 keV unabsorbed flux. Therefore we do not take absorption into account in the following calculations.

There is no significant dip in the data of LS 5039 at the phases close to superior conjunction. To put constraints on the binary parameters based on the lack of occultation only, we explore

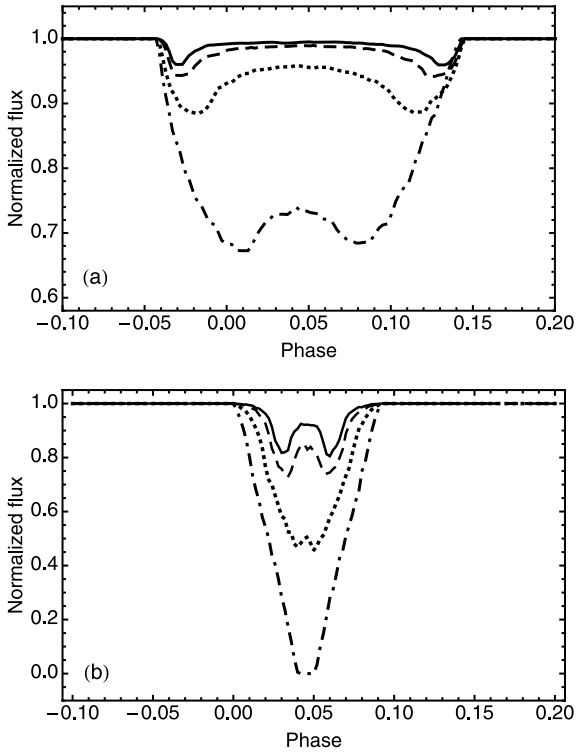


**Figure 4.** Light curves showing the effect of occultation in LS 5039 (a) $i = 60^\circ$ and $\eta_0 = 0.6$ and (b) $i = 90^\circ$ and $\eta_0 = 0.004$ (measured at periastron). The curves correspond to emitting regions with sizes $R_{out}$, $15R_\star$ (solid), $10R_\star$ (dashed), $5R_\star$ (dotted), $2R_\star$ (dot–dashed).

the parameter space to find solution to the equation in superior conjunction:

$$\frac{1}{N}\sum_{j=1}^{N}\zeta_j(i,\phi) = 1 - 3\sigma_d. \quad (12)$$

The final product of the study is Fig. 5 where areas above each curve correspond to inclination angles and sizes of the X-ray emitter for which the effect of occultation at superior conjunction does not exceed the $3\sigma_d$ limit. The range of allowed parameters changes with the shape of CD.

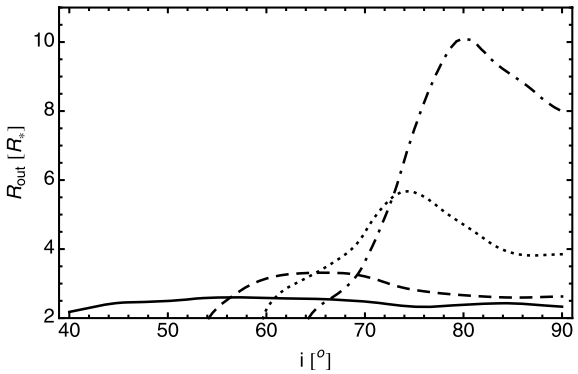


**Figure 5.** The areas above each curve correspond to permitted values of $i$ and $R_{out}$ for which effect of occultation at superior conjunction does not exceed the $3\sigma_d$ limit. Each curve corresponds to different value of $\eta_0$, solid 0.6, dashed 0.08, dotted 0.02, dot–dashed 0.004 measured at periastron.

Downloaded from https://academic.oup.com/mnras/article/411/1/193/1038827 by CNRS - ISTO user on 22 November 2021

## 5 CONCLUSIONS

Using a 3D model of a gamma-ray binary in the framework of the pulsar wind scenario, we tested the influence of X-ray absorption and occultation on the light curve and spectrum of LS 5039. We find that occultation cannot be responsible for the smooth X-ray orbital modulation in LS 5039, since this would require $\eta_0 > 1$. This appears unlikely because there is no sign in the UV lines (McSwain et al. 2004) that the O star wind is quenched on the hemisphere facing the compact object. Even for the most favourable conditions ($\eta_0 = \eta_{\max} \approx 0.6$ and large $i$) the duration of occultation never exceeds $\Delta\phi = 0.2$. The cause of the X-ray modulation has to be found elsewhere (Takahashi et al. 2009; Dubus, Cerutti & Henri 2010).

Constraints on the binary geometry are derived from the observed upper limit on the intrinsic column density and on the depth of the occultation dip. Limiting the effects of absorption and occultation requires the X-ray source to be extended. The minimum size of the X-ray emitting region, which depends on the stellar mass-loss rate, the shape of the CD and the inclination angle, varies between 3 and $15R_\star$. An emitter size $>4R_\star$ with $\eta_0 \gtrsim 0.02$ would be compatible with a 90° binary inclination. The limit based on the lack of X-ray eclipses and assuming a point source at the compact object location is 60° (Casares et al. 2005). A large X-ray source also loosens the constraints on the stellar mass-loss rate derived from the observed lack of intrinsic absorption. For example, for $\eta_0 \sim 0.004$, an emission region $\sim 3R_\star$ at inclination $\sim 50°$, allows a mass-loss rate of $1.5 \times 10^{-7}\,\mathrm{M_\odot\,yr^{-1}}$ compared to $4.7 \times 10^{-8}\,\mathrm{M_\odot\,yr^{-1}}$ for a point source located at the pulsar position. A more precise determination of the stellar wind mass-loss rate would greatly help narrow down the possibilities. Still, we can conclude that an extended X-ray source appears necessary to reconcile the pulsar wind scenario with the upper limits on X-ray absorption in the wind and the absence of occultation features in the light curve.

An extended X-ray source in gamma-ray binary can be expected in the pulsar wind scenario. High-energy electrons will be accelerated and randomized all along the termination shock of the pulsar wind. The shock distance from the pulsar is smaller towards the stellar companion than away from the O star, the efficiency of particle acceleration may also change at different locations. Calculations also show that the synchrotron emission from the electrons peaks in the 1–10 keV range only after significant cooling (Dubus 2006; Dubus, Cerutti & Henri 2008). For a typical magnetic field of 0.1–1 G, the injected electrons radiate primarily synchrotron above 0.1 MeV while they upscatter stellar photons to energies above a GeV. The electrons are advected away in the shocked flow with an initial speed $\approx c/3$. The bulk of the 1–10 keV radiation is emitted at a distance $\approx 3R_\star$ from the star in fig. 4 of Dubus (2006). More detailed modelling is required to obtain the exact evolution of the shock conditions with distance and quantify precisely the extent of the X-ray emission region. Such modelling would also yield the precise contribution to the X-ray emission and absorption from the shocked stellar wind region, which we have neglected here (Section 2).

The application to other known gamma-ray binaries is not straightforward since these contain a Be star with a dense equatorial outflow in addition to the tenuous stellar wind. The geometry of the interaction region with the pulsar wind changes between the polar wind and the equatorial wind and can have a complicated shape at the transition that has yet to be investigated. However, the wider orbits of LS I+61°303 and PSR B1259−63, the estimated inclination of 36° in PSR B1259-63, will limit the impact of absorption and occultation on the light curve.

## ACKNOWLEDGMENTS

This work was supported by the European Community via contract ERC-StG-200911 and in part by the Polish MNiSW grant NN203065933.

## REFERENCES

Abdo A. A. et al., 2009a, ApJ, 701, L123
Abdo A. A. et al., 2009b, ApJ, 706, L56
Aharonian F. et al., 2005, A&A, 442, 1
Aharonian F. et al., 2006, A&A, 460, 743
Aharonian F. A. et al., 2007, A&A, 469, L1
Albert J. et al., 2006, Sci, 312, 1771
Antokhin I. I., Owocki S. P., Brown J. C., 2004, ApJ, 611, 434
Aragona C., McSwain M. V., Grundstrom E. D., Marsh A. N., Roettenbacher R. M., Hessler K. M., Boyajian T. S., Ray P. S., 2009, ApJ, 698, 514
Bogovalov S. V., Khangulyan D. V., Koldoba A. V., Ustyugova G. V., Aharonian F. A., 2008, MNRAS, 387, 63
Bosch-Ramon V., 2010, in Martí J., Luque-Escamilla P. L., Combi J. A., eds, ASP Conf. Ser. Vol. 422, Studying the Structure of the Stellar Wind in LS 5039. Astron. Soc. Pac., San Francisco, p. 77
Bosch-Ramon V., Motch C., Ribó M., Lopes de Oliveira R., Janot-Pacheco E., Negueruela I., Paredes J. M., Martocchia A., 2007, A&A, 473, 545
Canto J., Raga A. C., Wilkin F. P., 1996, ApJ, 469, 729
Casares J., Ribó M., Ribas I., Paredes J. M., Martí J., Herrero A., 2005, MNRAS, 364, 899
Castor J. I., Abbott D. C., Klein R. I., 1975, ApJ, 195, 157
Cerutti B., Dubus G., Henri G., 2008, A&A, 488, 37
Dermer C. D., Böttcher M., 2006, ApJ, 643, 1081
Dubus G., 2006, A&A, 456, 801
Dubus G., Cerutti B., Henri G., 2008, A&A, 477, 691
Dubus G., Cerutti B., Henri G., 2010, A&A, 516, A18
Harding A. K., Gaisser T. K., 1990, ApJ, 358, 561
Hoffmann A. D., Klochkov D., Santangelo A., Horns D., Segreto A., Staubert R., Pühlhofer G., 2009, A&A, 494, L37
Kallman T., 2005, in Bull. American Astron. Soc., 37, 480
Kirk J. G., Ball L., Skjaeraasen O., 1999, Astroparticle Phys., 10, 31
Kishishita T., Tanaka T., Uchiyama Y., Takahashi T., 2009, ApJ, 697, L1
Kudritzki R., Puls J., 2000, ARA&A, 38, 613
Maraschi L., Treves A., 1981, MNRAS, 194, 1
McSwain M. V., Gies D. R., 2002, ApJ, 568, L27
McSwain M. V., Gies D. R., Huang W., Wiita P. J., Wingert D. W., Kaper L., 2004, ApJ, 600, 927
Mokiem M. R. et al., 2007, A&A, 473, 603
Morrison R., McCammon D., 1983, ApJ, 270, 119
Paredes J. M., Bosch-Ramon V., Romero G. E., 2006, A&A, 451, 259
Phinney E. S., Evans C. R., Blandford R. D., Kulkarni S. R., 1988, Nat, 333, 832
Puls J., Vink J. S., Najarro F., 2008, A&AR, 16, 209
Romero G. E., Christiansen H. R., Orellana M., 2005, ApJ, 632, 1093
Stevens I. R., Blondin J. M., Pollock A. M. T., 1992, ApJ, 386, 265
Szalai T., Kiss L. L., Sarty G. E., 2010, J. Phys. Conf. Ser., 218, 012028
Takahashi T. et al., 2009, ApJ, 697, 592
Tavani M., Arons J., Kaspi V. M., 1994, ApJ, 433, L37

## APPENDIX A: RANDOM GENERATION OF UNIFORMLY DISTRIBUTED POINTS ON THE 3D SURFACE

Here we explain how to generate a random sample of points uniformly distributed on a 3D surface $S$, symmetrical with respect to $x$-axis, described by a function $f(\rho)$ where $\rho = \sqrt{y^2 + z^2}$. We adopt an accept–reject algorithm commonly used for generating random samples drawn from an arbitrary distribution.

Downloaded from https://academic.oup.com/mnras/article/411/1/193/1038827 by CNRS - ISTO user on 22 November 2021

First, we generate $N$ random points distributed uniformly on the $y$-$z$ plane. The points are denoted in polar coordinates as $(\rho_1, \psi_1)$, $(\rho_2, \psi_2), \ldots, (\rho_N, \psi_N)$ where $\rho_i \in \langle 0, \rho_{max} \rangle$ and $\psi_i \in \langle 0, 2\pi \rangle$.

Second, we assign to each point a random number $w \in \langle 0, 1 \rangle$, where $w_1, w_2, \ldots, w_N$ are drawn from an uniform distribution. The $w_i$ are weights, used to accept and reject points on the basis of a density function

$$P(\rho_i) \sim \frac{dS}{M \rho_i \Delta\rho \Delta\psi} = \frac{1}{M}\sqrt{1 + \left(\frac{f(\rho_i + \Delta\rho) - f(\rho_i)}{\Delta\rho}\right)^2}, \quad \text{(A1)}$$

where $\Delta\rho \to 0, \mathrm{P}(\rho_i) \in \langle 0, 1 \rangle$, $dS$ is a unit 3D surface element given by equation (7), and

$$M = \sqrt{1 + \left(\frac{f(\rho_{max} + \Delta\rho) - f(\rho_{max})}{\Delta\rho}\right)^2}. \quad \text{(A2)}$$

Finally, from our sample of points uniformly distributed on the 3D surface, we choose only points for which $w_i < P(\rho_i)$. In the paper, $f$ is the solution to equation (5), while $\rho_{max}$ is determined by $R_{out}$ and has to be found numerically. An example sample of points is plotted in Fig. 2.

This paper has been typeset from a TEX/LATEX file prepared by the author.

Downloaded from https://academic.oup.com/mnras/article/411/1/193/1038827 by CNRS - ISTO user on 22 November 2021